Japanese Journal of Applied Physics
Vol. 44, No. 6A, 2005, pp. 3983–3991

Application of Photoalignment Technology to Liquid-Crystal-on-Silicon Microdisplays

Baolong ZHANG, KuenKuen LI, Vladimir G. CHIGRINOV, Hoi-Sing KWOK and Ho-Chi HUANG*

Department of Electrical and Electronic Engineering, The Hong Kong University of Science and Technology, Kowloon, Hong Kong, China

(Received November 30, 2004; accepted February 8, 2005; published June 10, 2005)

We applied photoalignment technology to liquid-crystal-on-silicon microdisplays and characterized their performance. A three-step photoexposure method was developed to solve problems with alignment disturbances on reflective silicon panels. The azimuthal and polar anchoring energies of photoalignment layers produced by this method were high and comparable with that of rubbed polyimide layers. We assembled both the rubbed and photoaligned microdisplays on a MTN 90° configuration for characterization and comparison. These two kinds of silicon microdisplays had good and comparable characteristics in terms of contrast, response time, voltage holding ratio and residual DC charge. The rubbed microdisplays were more uniform, which we attributed to a more mature fabrication technology, while the photoaligned microdisplays had far fewer defects due to the noncontact nature of the photoalignment technology. [DOI: 10.1143/JJAP.44.3983]

KEYWORDS: liquid crystal display, silicon microdisplay, LCOS, photoalignment

1. Introduction

Liquid-crystal-on-silicon (LCOS) microdisplays are advanced displays that integrate silicon very-large-scaled-integration (VLSI) circuits with thin-film-transistor liquid crystal displays (TFT-LCDs).[1–3] The LCOS microdisplays can have very high resolution and yet maintain a large aperture ratio or optical efficiency. Ancillary VLSI circuits such as display drivers or digital signal processors can be integrated into the display itself to produce a system on a chip. As more and more silicon microdisplay panels have been fabricated by sub-micron silicon VLSI technology for higher information content, the pixel pitch has been pushed down to below 10 μm.[4–6] A compatible liquid crystal assembly technology is needed in order to deal with the small dimensions of pixels, particularly for aligning small liquid crystal molecules efficiently on such small pixels.

The conventional process of aligning liquid crystal molecules on a silicon panel is by mechanical rubbing, which generates grooves in the rubbing direction on alignment layers of the silicon surface. The liquid crystal molecules are then aligned into these grooves during a later liquid crystal filling process. However, the grooves generated by mechanical rubbing are much larger than liquid crystal molecules. Alignment of liquid crystal molecules in these grooves may be perturbed, and a portion of liquid crystal molecules may not be aligned exactly in the rubbing direction. This inefficient alignment of liquid crystal molecules reduces contrast in the display. The misaligned area may occupy a large portion of small pixels and result in speckles on the display. These small speckles are not observable in a direct-view LCD. However, they are not negligible and present a major defect in LCOS microdisplays where small pixels are projected or magnified for viewing. In addition, mechanical rubbing on a silicon surface may generate dust, electrostatic charges and scratches, and further reduce the yield of LCOS microdisplays.

Photoalignment is a noncontact method and shows promise for solving the above-mentioned problems.[7,8] Instead of physical rubbing, a polarized UV light is illuminated on a photosensitive layer of the silicon surface. Through both photochemical and photophysical transformations in this photosensitive layer, a very fine alignment mechanism can be established on the photosensitive layer for precise alignment of liquid crystal molecules. This alignment mechanism is due to Van der Waals interactions on the surface and can be very fine. In addition, high pretilt angles of the alignment layer can be obtained by controlling the illumination angles and doses of polarized UV light. Associated with the high pretilt angles are the advantages of the method's fast switching time and low threshold voltage.

In our previous work, we synthesized a variety of photoalignment materials using azo dyes.[7] Photoalignment of these azo dye layers takes place purely due to reorientation of molecular absorption oscillators, which are perpendicular to the polarization of the incident UV light. We have applied these azo dye photoalignment layers to plain liquid crystal cells and developed a two-step photoexposure method to obtain a temperature stable pretilt angle of 5.3°.[7] The first exposure is a normal incident and linearly polarized light to activate reorientation of these molecules, and the second exposure is an oblique nonpolarized light to generate pretilt angles. We found that these photoaligned liquid crystal cells had a higher voltage holding ratio than the conventional rubbed cells. This enables the application of this family of azo dyes as alignment layers in active matrix liquid crystal displays (AMLCDs).

In this study, we applied this photoalignment technology to LCOS microdisplays and characterized their performance. We used azo dye SD1, which provided the best alignment of liquid crystal molecules in our previous findings, as the photosensitive layer.[9] We applied this photosensitive layer to a 0.56-inch silicon microdisplay panel, and then assembled this panel on a mixed-mode twisted (MTN) liquid crystal configuration[10] for characterization. Both the photoalignment and rubbing methods were used for comparison.

2. Photoalignment Materials and Silicon Panels

2.1 Photoalignment materials

We used azo dye SD1 as the photoalignment material. The dye molecules were first synthesized by azo-coupling between 2,2′-benzidine disulfonic acid and salicylic acid. The synthesized molecules were then purified by recrystallization. The chemical structure of azo dye SD1 is shown in Fig. 1.

Figure 2 shows absorption spectra of a 100 Å SD1 layer

*Author for correspondence. E-mail address: eehuang@ust.hk

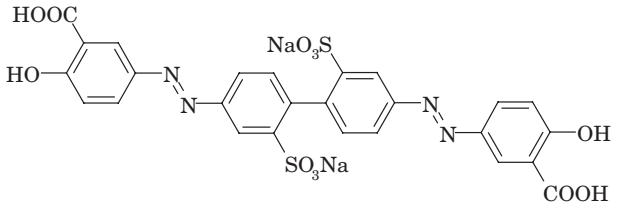

Fig. 1. Chemical structure of photoalignment material SD1.

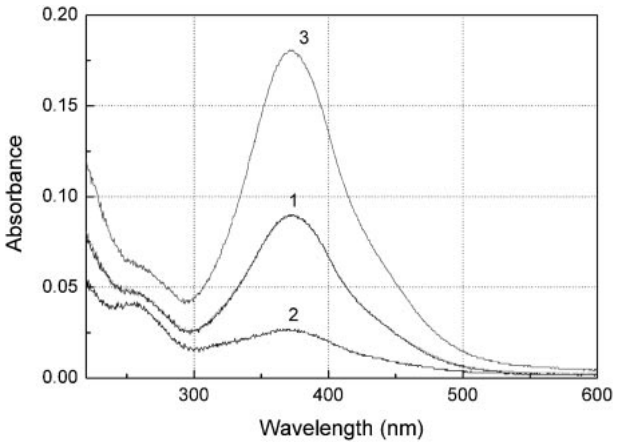

Fig. 2. Absorption spectra of 100 Å SD1 layer before and after UV light exposure.

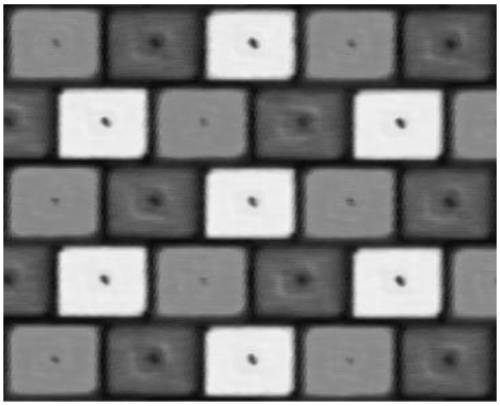

Fig. 3. Pixel array coated with red, green and blue micro-color filters.

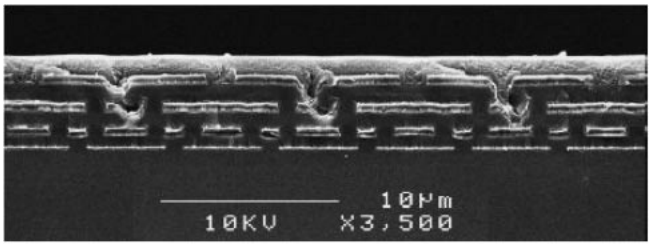

Fig. 4. SEM image of cross section of a color silicon panel.

before and after UV light exposure of $1\,\mathrm{J/cm^2}$. Whereas, curve 1 was recorded before the UV light exposure; curve 2 after exposure to parallel linearly polarized UV light; and curve 3, after exposure to perpendicular linearly polarized UV light. A UV/vis spectrophotometer from Perkin Elmer was used for these measurements. The intensity of the absorption spectrum of SD1 decreased after SD1 was exposed to parallel linearly polarized UV light, as shown in curve 2. On the other hand, the intensity of the absorption spectrum increased after SD1 was exposed to perpendicular linearly polarized UV light, as shown in curve 3. We defined an order parameter to express the magnitude of absorption in parallel and perpendicular directions as follows:[7)]

$$S = \frac{A_{\parallel} - A_{\perp}}{A_{\parallel} + 2A_{\perp}}, \tag{1}$$

where $A_{\parallel}$ and $A_{\perp}$ are absorption coefficients of the SD1 film after exposure to parallel and perpendicular linearly polarized UV light, respectively. The order parameter increased with exposure time and dose of the linearly polarized UV light, and eventually saturated at a maximum value of $S_{\max} = -0.5$. The order parameter S of SD1, as characterized and shown in Fig. 2, is -0.4 at a maximum absorption wavelength, $\lambda_{\max}$, of 372 nm.

2.2 Silicon panels

We used 0.56-inch silicon panels as substrates to assemble LCOS microdisplays. The silicon panel had $688 \times 480 \times 3$ spatial resolutions and was designed and fabricated by a 3.3/15 V dual-voltage LCD driver process. The 3.3 V is for data logic and the 15 V is to drive the liquid crystal layer on top of the silicon panels. In this design, pixels were arranged in delta shapes and micro-color filters were coated on these pixels to render color. Figure 3 shows the pixel array coated with red, green and blue micro-color filters, where the pixel pitch was $8.4 \times 11.2\,\mu\mathrm{m}^2$. It is therefore advantageous to have a noncontact or photoalignment method for alignment of liquid crystal molecules on this fine pixel array. The mechanical rubbing tends to rub away micro-color filters and causes pinholes and point defects.

The micro-color filter array could also serve as a passivation layer to improve the surface flatness of the silicon panel. Figure 4 shows a SEM image of a cross section of this color silicon panel. The topographic variation of the silicon surface was 4000 Å before micro-color filters were employed. After coating and re-flowing of a layer of 6000 Å micro-color filters on the silicon surface, the topographic variation of the pixel array was reduced to 500 Å. In this case, the 4000 Å valleys of pixel gaps were filled with overlapping micro-color filters.

3. Photoaligned Silicon Microdisplays

3.1 Photoalignment layers

With silicon panels and photoalignment materials prepared, we were ready to assemble photoaligned LCOS microdisplays. The azo dye SD1 photoalignment material was first dissolved in *N*,*N*-dimethylformamide (DMF) to a concentration of 1% by weight. The solution was then spin-coated on both silicon panels and indium–tin-oxide (ITO) glass substrates. Thereafter, the silicon panels and glass substrates were baked on a hot plate at 100°C for 10 min to remove solvents and improve adhesion.

It is important to have the same thickness of spin-coated photoalignment layers on both the silicon panel and the glass substrate for later photoexposure. However, the surface of

the silicon panel was much rougher than that of the ITO glass substrate because of wafer fabrication. In order to achieve the same thickness, the spin rate for silicon panels had to be slightly faster than that for glass substrates. In our experiments, we used 4000 rpm for silicon panels and 3500 rpm for glass substrates to obtain 100 Å thick azo dye layers on both the substrates. We could also increase the thickness from 100 to 300 Å by reducing the spin rates from 4000 and 3500 rpm to 2000 and 1800 rpm, respectively.

3.2 Two-step photoexposure for glass substrates

After the application of a thin photoalignment layer on both silicon panels and glass substrates, linearly polarized UV light was irradiated onto the photoalignment layers on both substrates. We used a super high-pressure Hg lamp as a light source and an interference filter at 365 nm as well as a wire grid polarizer to obtain output as linearly polarized UV light. The wavelength is close to the maximum absorption wavelength, $\lambda_{max} = 372$ nm, of SD1. We developed a two-step photoexposure method to activate photoalignment films on glass substrates in our previous work.[7] In this work, we adopted the same procedure to activate photoalignment films on glass substrates. Figure 5 illustrates this two-step photoexposure procedure for glass substrates.

At first, s-polarized UV light at 4.8 mW/cm^2 was irradiated in a perpendicular direction with respect to the photoalignment layer on the glass substrates for 3.4 min, or for 1 J/cm^2, as shown in Fig. 5(a). This exposure initiated reorientation of the azo dye SD1 molecules and changed their random azimuthal orientations to a uniform orientation.

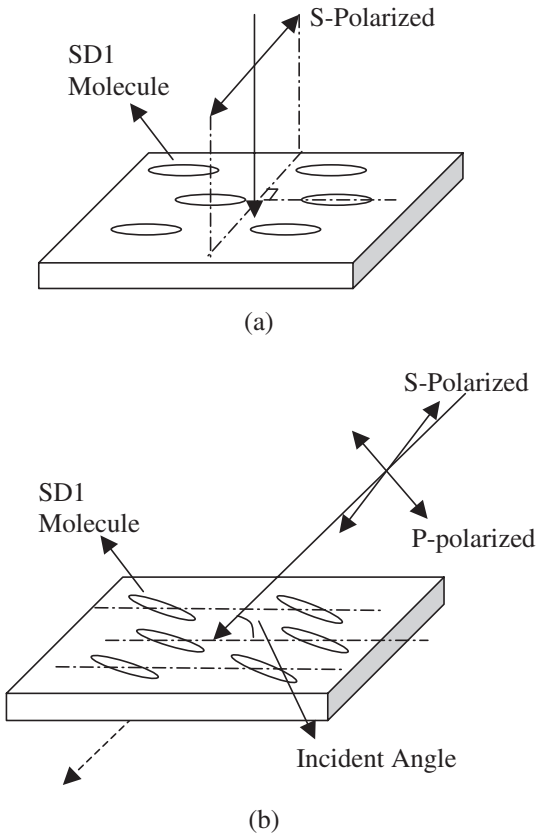

Fig. 5. Two-step photoexposure procedure for glass substrates: (a) normal exposure and (b) oblique exposure.

The new orientation was perpendicular to the polarization of the incident UV light. Fine alignment structures due to Van der Waals interactions in the photoalignment layer were created after this exposure. This layer was still not suitable to align liquid crystal molecules because the surface was still rough in the alignment direction. A second exposure was needed to smooth out the roughness and create uniform pretilt angles.

The second exposure was an oblique nonpolarized UV light at 40 mW/cm^2 for 7 min, or for 16.8 J/cm^2, as shown in Fig. 5(b). The s-polarized portion of light, which is parallel to the glass substrate, further aligned the azo dye SD1 molecules just as it did in the first step. The p-polarized portion of light caused the azo dye molecules to rotate and create pretilt angles on the surface. The pretilt angle increased with exposure time and eventually saturated. In the experiment, we used an oblique incident angle of 45° and obtained a pretilt angle of 5.3° on the 100 Å azo dye SD1 layer. This pretilt angle was stable after a hot bake at 100°C on a hot plate for 10 min.

We applied the same two-step photoexposure procedure to photoalignment layers on silicon panels, but the results were very different. The silicon panel is reflective. The incident s-polarized UV light, after passing through the azo dye SD1 layer, bounced back and activated the alignment layer one more time. As a result, the energy applied to the photoalignment layer was twice that of the first-step exposure of normal incidence. For the second-step exposure of oblique incidence, the incident p-polarized light rotated the pretilt angle in one direction, while the reflected p-polarized light would rotated the pretilt angle in the opposite direction. This reflected p-polarized light would therefore offset the pretilt angle generated by the incident p-polarized light. As a result, the pretilt angles on the SD1 layer remained amorphous.

We applied the two-step photoexposure method to both the silicon panel and the glass substrate and assembled a 90° mixed-mode twisted nematic (MTN) cell with these two substrates. The cell was uniform and the alignment was good when no voltage was applied. When we applied a voltage to transit the LC cell from nonselected to selected states, alignment defects appeared. Figure 6 shows appearance of the LC cell during transitions. Because pretilt angles were small and were perturbed on the silicon panel, no preferred direction existed in which liquid crystal molecules tilted up. As a result, reverse tilt domains occurred and were dispersed

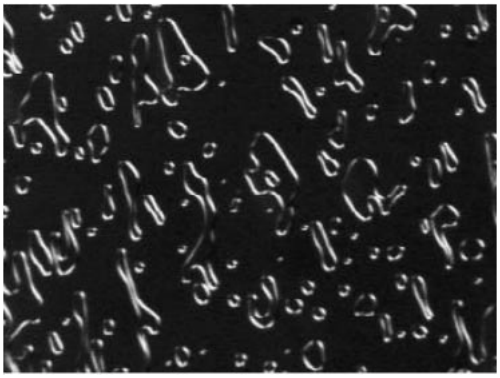

Fig. 6. Alignment defects in silicon microdisplay because of two-step photoexposure.

randomly in the LC cell. These appearances lasted for a few seconds and then disappeared when the LC cell gradually changed to a homogeneous state because of elastic deformation. This is an undesired effect and must be eliminated. A new photoexposure mechanism is needed to solve this problem.

3.3 Three-step photoexposure for silicon panels

The most straightforward approach to solve this problem is to reduce the reflected p-polarized light. This can be achieved by determining an optimal oblique incident angle such that the reflected p-polarized light is minimized for a given thickness of the photoalignment layer. The other possibility is to increase the thickness of the azo dye SD1 layer to absorb more incident UV light, so the reflected p-polarized light is negligible in comparison with the incident p-polarized light.

We modeled the UV light irradiation on the reflective silicon panel using a 4×4 matrix[11] as follows:

$$\begin{pmatrix} I_s \\ R_s \\ I_p \\ R_p \end{pmatrix} = M \begin{pmatrix} T_s \\ 0 \\ T_p \\ 0 \end{pmatrix}, \tag{2}$$

where I_s and I_p are incident s-polarized and p-polarized light, respectively; R_s and R_p are reflected s-polarized and p-polarized light, respectively; T_s and T_p are transmitted s-polarized and p-polarized light, respectively. M is the transfer matrix of the SD1 and aluminum layers and can be expressed as:

$$M = D_{air}^{-1} \cdot D_{SD1} \cdot P_{SD1} \cdot D_{SD1}^{-1} \cdot D_{Al} \cdot P_{Al}, \tag{3}$$

where D_{air}, D_{SD1} and D_{Al} are dynamic matrices of air, SD1 and aluminum, respectively; and P_{SD1} and P_{Al} are propagation matrices of SD1 and aluminum layers, respectively. The wavelength used in these two equations was 365 nm; this was light from the Hg UV lamp after passage through an interference filter of 365 nm. At this wavelength, the refractive indices of air, SD1 and aluminum are available and are listed in Table I.[7,12]

With this 4×4 matrix model, we simulated reflected s- and p-polarized light with respect to incident angles. The simulation results are shown in Fig. 7. Curves (a) and (b) are the normalized reflectances of s- and p-polarized light for a 100 Å SD1 layer, respectively. Curves (c) and (d) are the normalized reflectances of p- and s-polarized light for a 300 Å SD1 layer, respectively.

The reflectance of p-polarized light for the 100 Å SD1 layer was always larger than that for the 300 Å layer because the thicker layer absorbed more light. A minimal reflectance occurred at incident angles of 70° and 65° for the 100 Å and 300 Å layers, respectively. For the second exposure of silicon panels, we irradiated UV light to the 100 Å and 300 Å SD1 layers at incident angles of 70° and 65°, respectively, and obtained a 4.1° pretilt angle for the 100 Å layer and a 5.7° pretilt angle for the 300 Å layer. These pretilt angles are comparable to those generated by mechanical rubbing. Figure 8 shows a schematic of the three-step photoexposure on a silicon panel.

Table I. Refractive indices of air, SD1 and aluminum.

	n	Δn	k	Δk
Air	1	0	0	0
SD1	1.8	0.03	0.67	1
Aluminum	0.4	0	3.92	0

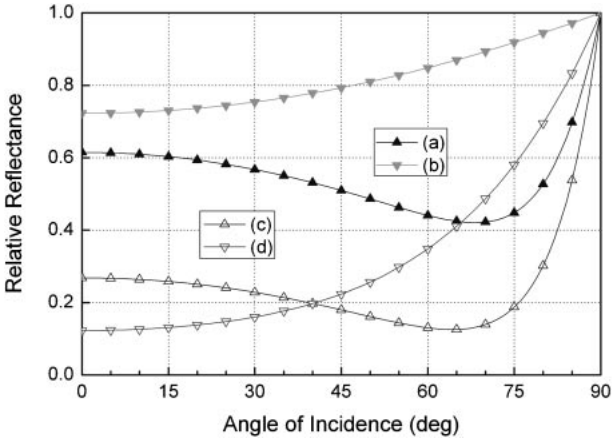

Fig. 7. Simulated results of s- and p-polarized light on silicon panels.

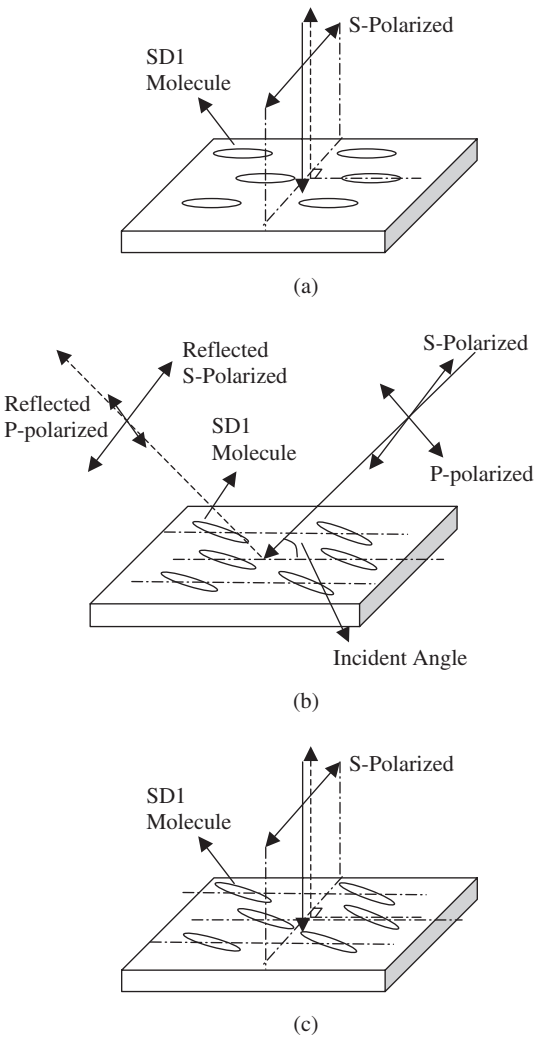

Fig. 8. Schematic of three-step photoexposure on silicon panel: (a) normal exposure, (b) oblique exposure and (c) normal exposure.

Table II. Five silicon microdisplays with different alignment layers.

	Alignment layer on	
	Glass substrate	Silicon substrate
Microdisplay A	AL5056	AL5056
Microdisplay B	AL5056	100 Å SD1
Microdisplay C	100 Å SD1	AL5056
Microdisplay D	100 Å SD1	100 Å SD1
Microdisplay E	300 Å SD1	300 Å SD1

Although we tried to minimize the reflected p-polarized light in the second exposure, a small amount of p-polarized light still existed and perturbed the alignment of SD1 molecules. As a result, alignment defects were generated on the SD1 layer and reduced the in-plane order parameter during the second exposure. A third exposure of s-polarized UV light at normal incidence, as shown in Fig. 8(c), could further improve the in-plane order parameter and hence the alignment efficiency. In this step, a low energy dose of 0.3 J/cm^2 was adequate to anneal the alignment defects caused by reflection of p-polarized UV light during the second exposure.

3.4 Reflective liquid crystal modes

We applied the two-step photoexposure method to glass substrates and the three-step method to silicon panels. Afterwards, we assembled the two substrates on an MTN reflective liquid crystal mode configuration, in which the twist angle was 90°, the polarizer angle was 20° and the retardation was 0.25 μm.[10] We used the LC88Y1104 liquid crystal mixture ($\Delta n = 0.0752$) from Merck and the cell gap was 3.3 μm. For comparisons we also prepared silicon microdisplays by rubbing, in which AL5056 polyimide from JSR was used for the alignment layers. Table II summarized these five silicon microdisplays with different alignment layers.

4. Characterization of Silicon Microdisplays

4.1 Anchoring energy of photoalignment layers

In addition to pretilt angle, anchoring energy is another important figure of merit for alignment layers. We measured the azimuthal anchoring energy of the SD1 layer on silicon panels using a torque balance method.[13] Microdisplay B, which had rubbed polyimide on a glass substrate and a photoaligned SD1 layer on a silicon panel, was used for this measurement. The twist angle of Microdisplay B can only achieve a value of 90° if there is a sufficiently large anchoring energy on the photoaligned silicon panel. Otherwise, the twist angle decreases due to elastic torque produced by the rubbed polyimide on the glass substrate where the anchoring energy is considered to be strong.[7] The azimuthal anchoring energy A_φ of the SD1 layer on a silicon panel can be calculated from the following torque balance equation:

$$A_\varphi = \frac{2K_{22}\varphi_m}{d\sin(\Phi - \varphi_m)}, \tag{4}$$

where Φ is the desired twist angle of 90°, φ_m is the measured twist angle, K_{22} is the twist elasticity constant of liquid crystal with a value of 8.4×10^{-12} N, and d is the cell gap of 3.3 μm. We measured the twist angle by spectroscopic ellipsometry[14] with an accuracy of 1°. The measured twist angle, φ_m, was larger than 89° and close to 90°. The calculated azimuthal anchoring energy A_φ was therefore larger than 4×10^{-8} J/cm^2, which is comparable to that of the rubbed polyimide layer.

In addition, we also measured the twist angle of Microdisplay C, which has a photoaligned SD1 layer on a glass substrate and rubbed polyimide on a silicon panel. The measured twist angle was also larger than 89° and close to 90°. These two measurements showed that the photoaligned SD1 layer indeed had a strong azimuthal anchoring energy, comparable to that of a rubbed polyimide, whether it was on silicon panels or glass substrates.

We used a differential method to measure the polar anchoring energy of SD1 layers on silicon panels.[9] Figure 9 illustrates the setup for this measurement. At first, we measured the retardation by an empty microdisplay, as shown in Fig. 9(a). From this measurement we obtained a base retardation value of the empty microdisplay. Then we filled the microdisplay and remeasured its retardation at different voltages, as shown in Fig. 9(b). The polar anchoring energy is a function of retardation and voltage as follows:

$$\frac{R}{R_0} = \frac{C_0 V_C \,\mathrm{const}}{CV} - 2\frac{K_1}{W_p d}, \tag{5}$$

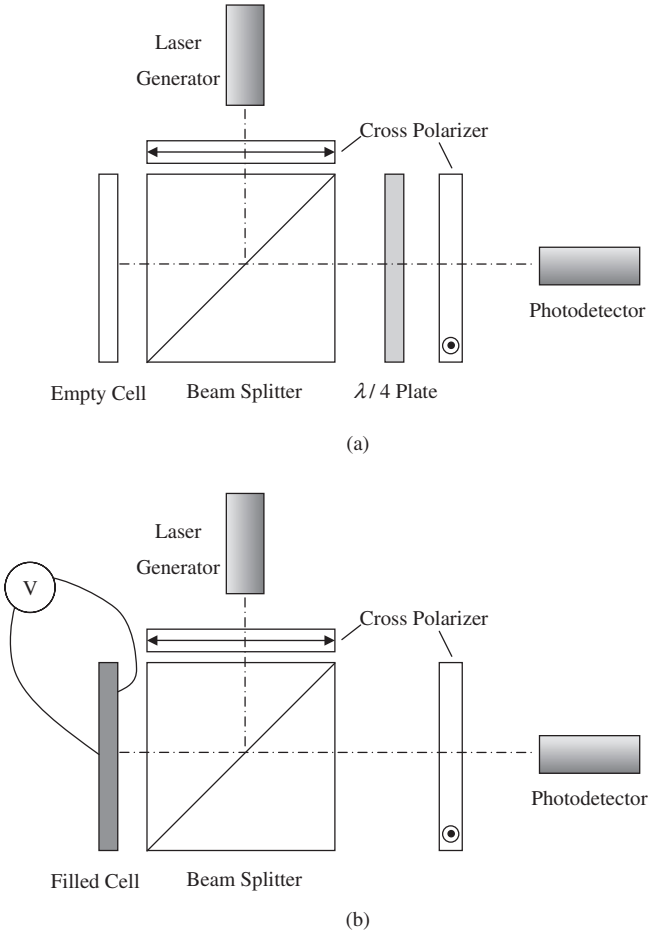

Fig. 9. Optical setup for measuring polar anchoring energy: (a) with empty cell and (b) with filled microdisplay.

where W_p is the polar anchoring energy, d is LC layer thickness, $K_1 = 7.3 \times 10^{-12}$ N is the LC splay elastic constant, C and C_0 are capacitances of the LC layer under the applied voltage V and infinite voltage, respectively, and V_C is the threshold voltage. When the applied voltage approaches infinity, the polar anchoring energy is reduced to the following:

$$R_{(1/V\to 0)} = -4\pi \frac{\Delta n}{\lambda} \frac{K_1}{W_p}, \tag{6}$$

where we substituted $R_0 = 2\pi\Delta nd/\lambda$ for d. The central wavelength of laser used in measurement is $\lambda = 632.8$ nm. At this voltage, all the liquid crystal molecules should tilt up to the maximum value that the polar anchoring energy of the alignment layer can support. From the retardation measured at this infinitely high voltage, we derived the polar anchoring energy using eq. (6).

We used photoaligned microdisplays for this measurement and measured their retardation from 5 to 40 V. The retardation was decreased from 0.175 μm at 5 V to 0.005 μm at 40 V and then gradually saturated. We extrapolated this curve to an infinitely high voltage and obtained a retardation of 1.7×10^{-3} μm, which corresponds to a polar anchoring energy of 5×10^{-8} J/cm^2 for the SD1 photoaligned layer. This value is not as high as that of a rubbed polyimide layer, which is typically 10×10^{-8} J/cm^2, but it is large enough for AMLCD applications, for which $(1–10) \times 10^{-8}$ J/cm^2 is suggested.[15)]

4.2 *Contrast and response time*

The most important parameters of silicon microdisplays are contrast and response time. We measured reflectance versus voltage and response time of microdisplay samples with a projector, as shown in Fig. 10. The setup used an F# = 2.0 optics and had a system contrast of 400. Figure 11 shows simulated and measured reflectance-versus-voltage curves for different microdisplays.

It can be seen from the figure that these curves have essentially the same shape. However, the curve for Microdisplay A is shifted to the right, while the curve of Microdisplay E is shifted to the left. As a consequence, the contrast of Microdisplay A at 3 Vrms was only 35 : 1, lower than the 180 : 1 of Microdisplay D and the 280 : 1 of Microdisplay E.

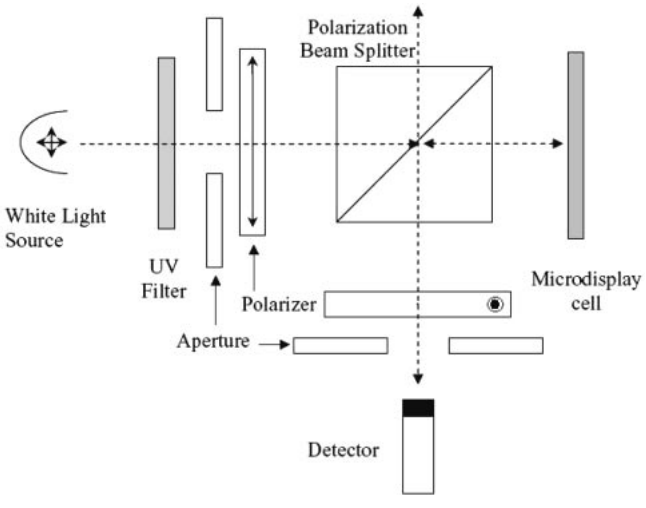

Fig. 10. Optical setup for measuring RVC curve and response time.

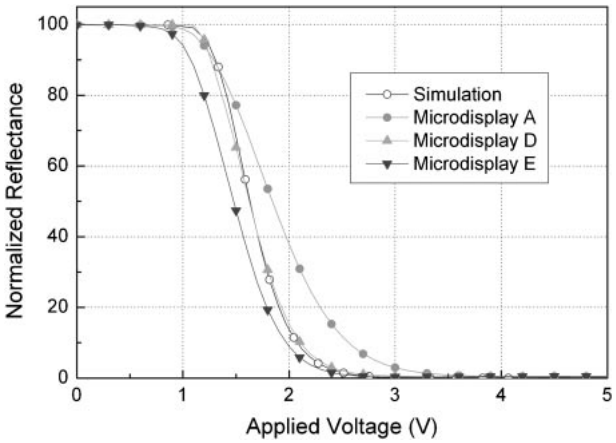

Fig. 11. Simulated and measured reflectance-versus-voltage curves for different microdisplays.

Pretilt angles account for the shift of these curves. A higher pretilt angle lowers the threshold voltage and hence shifts the reflectance-versus-voltage curve to lower voltage or to the left. The pretilt angles of photoaligned Microdisplay D and E were 4.1° and 5.7°, respectively. Pretilt angles in this range can also be obtained by mechanical rubbing. For a rough silicon surface, however, we had to rub polyimide layers more heavily on silicon panels to ensure adequate anchoring energy. As a result, the pretilt angle on the silicon panels was reduced to 2.5° because of the heavier rubbing. The reflectance-versus-voltage curve of Microdisplay A was therefore shifted to the right due to a larger threshold voltage. In comparison, the reflectance-versus-voltage curve of Microdisplay E was shifted to the left or to lower voltage, because it had the largest pretilt angle and the lowest threshold voltage.

In addition to the shift in the threshold voltage, the slope of the reflectance-versus-voltage curves also differed slightly among these microdisplays. Microdisplay E has the most abrupt curve, while Microdisplay A has a smooth curve with voltage. We attributed this difference to polar anchoring energy. The photoalignment layer has a lower polar anchoring energy than that of a rubbed polyimide. It is easier to tilt up liquid crystal molecules in photoaligned microdisplays. As a result, the change in reflectance is more abrupt with voltage and the reflectance-versus-voltage curve is steeper.

Figure 12 shows measured response times for Microdisplays A, D and E. It was observed again that Microdisplay E, which has the lowest threshold voltage, had a fast response time from either nonselected to selected (NS) states, or from selected to non-selected (SN) states. The NS and SN response times of Microdisplay E were less than 1 ms and 9 ms, respectively. The response time of Microdisplay D was slightly longer than that of Microdisplay E, but was still comparable to that of Microdisplay A. In short, the response times for these three microdisplays are fast enough for video applications.

4.3 *Voltage holding ratio and residual DC charge*

We also measured the voltage holding ratio (VHR) and

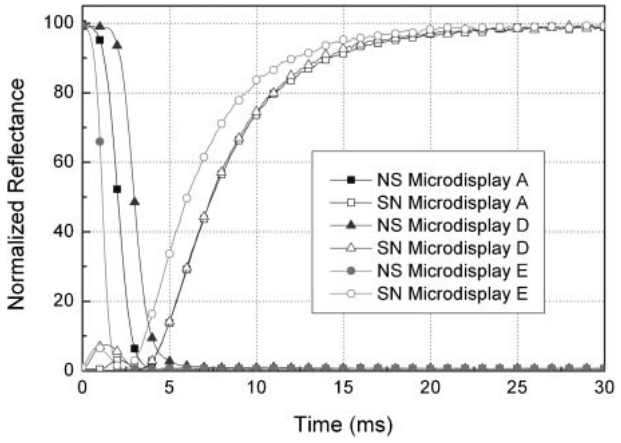

Fig. 12. Response time for Microdisplays A, D and E.

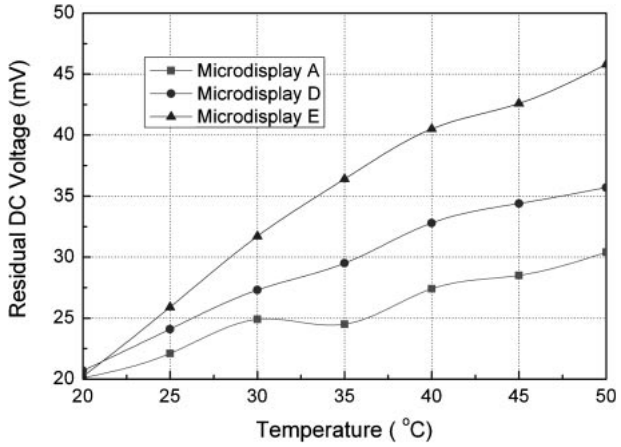

Fig. 14. RDC voltages of Microdisplays A, D and E from 20 to 50°C.

the residual DC (RDC) charge for polyimide-rubbed Microdisplay A and photoaligned Microdisplays D and E. The VHR of silicon microdisplays depends mainly on the specific resistivity of liquid crystal mixtures and the voltage holding capability of silicon pixels.[16] The thin alignment layer should have no significant effect on VHR as long as it does not diffuse out and contaminate the liquid crystal mixtures. The VHR measurement was carried out to probe the pixel voltage directly. A short voltage pulse was applied to a pixel during the address time, and the charged pixel voltage was preserved by the pixel until the next refresh. We buffered and amplified this pixel voltage using a high-impedance operational amplifier and recorded the amplified voltage using a digital oscilloscope.

Figure 13 shows the VHR measurements of these three microdisplays at room temperature (25°C). The pixel voltage of Microdisplay A decayed by 60 mV from a peak of 2.0 V over a period of 16.7 ms or at 30 Hz AC frequency. We defined the VHR as the ratio of the root-mean-square voltage divided by the applied voltage pulse on the probed pixel. The 30 Hz VHR for Microdisplay A was therefore 98.5%. Similarly, we calculate the VHR for Microdisplays D and E from the curves in Fig. 13. Both values were slightly larger than 98% at 25°C, and we considered them good with respect to AMLCD standards. The high VHR of photoaligned microdisplays also indicated that the azo dye layer was chemically stable and did not diffused out into the liquid crystal mixtures to cause contamination.

In addition to VHR, RDC charge is another important parameter for silicon microdisplays which have different electrodes on silicon panels and glass substrates. The ITO electrodes on glass substrates and aluminum pixels on silicon panels have different work functions, are ions in polar liquid crystal molecules are attracted and accumulated on the silicon pixels. The alignment layer has direct contact with liquid crystal mixtures, and silicon pixels might further trap these charges on their surface and increase the RDC charge.

RDC measurements were used to evaluate RDC charge on a silicon surface. A square wave was applied to Microdisplays A, D and E at temperatures from 20 to 50°C, and a photodetector connected to a digital oscilloscope was used to monitor the reflectance of these microdisplays. Flickering was recorded and the DC offset voltage was varied in 10 mV steps until the flicker was minimized. This DC offset voltage was recorded as the RDC voltage.

Figure 14 shows measured RDC voltages of Microdisplay A, D and E from 20 to 50°C. The RDC voltage showed a slight temperature dependence and increased from 20 to 30 mV in Microdisplay A. The AL5056 polyimide in Microdisplay A had a low charge accumulation potential;[17] and hence it did not accumulate significantly RDC charges. The photoaligned Microdisplays D and E had larger RDC charges than the rubbed Microdisplay A. Microdisplay E had the largest RDC charge, which was attributed to the thicker SD1 layer having more interfacial states that trap more RDC charges. All RDC voltages of these three microdisplay samples at room temperature were below 50 mV, which was considered as an acceptable RDC voltage for an AMLCD.

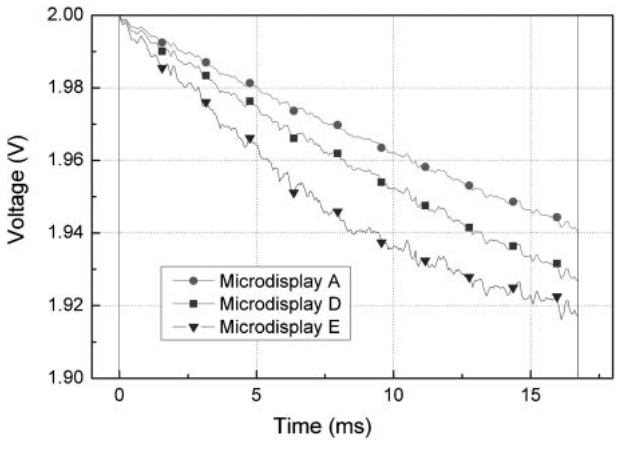

Fig. 13. VHR measurements of Microdisplays A, D and E at 25°C.

4.4 Overall performance of silicon microdisplays

We turned on the microdisplays and examined their overall performance. A white light-emitting diode (LED) through a simple collimating lens was used to illuminate the microdisplays. Figure 15 shows magnified images of the rubbed Microdisplay A and the photoaligned Microdisplay E, respectively. Both images reveal good contrast and color saturation, which indicates that the LC alignment in both the displays was good. However, Microdisplay A is

(a)

(b)

Fig. 15. Magnified images of (a) rubbed Microdisplay A and (b) photoaligned Microdisplay E.

more uniform than Microdisplay E. Microdisplay A had 92% uniformity according to 9-point measurements, while Microdisplay E had only 81% uniformity. We believed this nonuniformity of the photoaligned microdisplay was caused by our immature fabrication capability during the photoalignment process. All nonuniform photoalignment materials, spin-coat processes and UV light exposures contributed to the nonuniformity of the photoalignment layer on the microdisplay. In the contrast, we had dedicated equipment for applying and rubbing more matured polyimide film more uniformly across the entire display area. Consequently, we were able to produce a more uniform rubbed microdisplay.

We also examined Microdisplays A, D and E with a 500× microscope for their defects. Figure 16 shows peeling of micro-color filters on the rubbed Microdisplay A, on which we had applied typical rubbing force to both the silicon panels and glass substrates. The situation was even worse

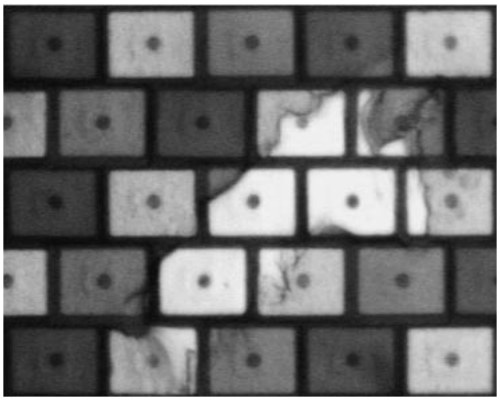

Fig. 16. Peeling micro-color filters on rubbed Microdisplay A.

when we increased the rubbing force by a factor of two on the rough silicon surface to obtain a stronger anchoring energy. In comparison, we did not observe any peeling of micro-color filters on photoaligned Microdisplays D and E.

Both the rubbed and photoaligned methods have their own strengths and weaknesses. The rubbing method is more mature and simpler in fabrication. The photoaligned method is still in its infancy. It is more complicated in fabrication, but promises to further improve the alignment efficiency of a display. From the characterizations that we have performed thus far, both the rubbed and photoaligned microdisplays have comparable characteristics. They all meet AMLCD standards. The most important advantage of the photoaligned method is its noncontact nature, which prevents defects caused by mechanical rubbing.

5. Conclusions

In this paper, we have reported the application and characterization of photoalignment layers on silicon microdisplays. We developed a three-step photoexposure method on reflective silicon panels to create pretilt angles on photoalignment layers. Both the azimuthal and polar anchoring energies of photoalignment layers, produced by this three-step photoexposure method, were high and comparable to those of rubbed polyimide layers. We assembled both the photoaligned and rubbed microdisplays on an MTN 90° configuration for characterization and comparison. It was observed that both the rubbed and photoaligned microdisplays had comparable characteristics. They all showed good contrast due to good alignment of liquid crystal molecules. They all had a response time of about 10 ms, which is fast enough for video applications. The VHR and RDC of both photoaligned and rubbed microdisplays were essentially the same and met AMLCD standards. However, it was noted that the rubbed microdisplays were more uniform, which we attributed to the more mature rubbing technology. It was also observed that defects were greatly reduced in photoaligned microdisplays due to the noncontact nature of the photoalignment technology.

Acknowledgement

This work was sponsored by a grant from the Research Grant Council of the Government of the Hong Kong Special Administrative Region of the People's Republic of China.

1) H. C. Huang, P. W. Cheng, W. C. Yip, H. S. Kwok, C. S. Li and Y. Liao: Conf. Rec. Int. Display Research Conf., 1995, p. 481.
2) P. M. Alt and K. Noda: IBM J. Res. Dev. **42** (1998) 315.
3) H. Kurogane, K. Doi, T. Nishihata, A. Honma, M. Furuya, S. Nakagaki and I. Takanashi: SID Symp. Dig. **29** (1998) 33.
4) H. C. Huang, D. D. Huang and J. Chen: Jpn. J. Appl. Phys. **39** (2000) 485.
5) A. Yumoto, M. Mano and M. Yamagishi: Proc. 7th Int. Display Workshops, 2000, p. 183.
6) J. Choi: Microdisplay Rep. **6** (2003) 1.
7) H. Akiyama, T. Kawara, H. Takada, H. Takatsu, V. Chigrinov, E. Prudnikova, V. Kozenkov and H. S. Kwok: Liq. Cryst. **29** (2002) 1321.
8) H. Seiberle, O. Muller, G. Marck and M. Schadt: Conf. Rec. 20th Int. Display Research Conf., 2000, p. 38.
9) V. Chigrinov, A. Muravski, H. S. Kwok, H. Takada, H. Akiyama and H. Takatsu: Phys. Rev. E **68** (2003) 061702.
10) S. T. Wu and C. S. Wu: Appl. Phys. Lett. **68** (1996) 1455.
11) P. C. Yeh: *Optical Waves in Layered Media* (Wiley, New York, 1988) Chap. 9, p. 239.
12) M. Bass, W. Van Stryland, R. Williams and L. Wolfe: *Handbook of Optics* (McGraw-Hill, New York, c1995–c2001) p. 1107.
13) Y. Iimura, N. Kobayashi and S. Kobayashi: Jpn. J. Appl. Phys. **33** (1994) L434.
14) S. T. Tang and H. S. Kwok: J. Appl. Phys. **89** (2001) 80.
15) Vladimir G. Chigrinov: *Liquid Crystal Device: Physics and Applications* (Artech House, London, 1999) Chap. 1, p. 77.
16) H. C. Huang and P. W. Cheng: Jpn. J. Appl. Phys. **40** (2001) 3448.
17) JSR Polyimide Catalog.